Chemical Physics Letters 771 (2021) 138465

Contents lists available at ScienceDirect

Chemical Physics Letters

journal homepage: www.elsevier.com/locate/cplett

Research paper

Predicting the energetic stabilization of Janus-MoSSe/AlN heterostructures: A DFT study

Ramiro M. dos Santos [a], Marcelo L. Pereira Júnior [a], Luiz F. Roncaratti [a], Luiz A. Ribeiro Júnior [a,b,*]

[a] Institute of Physics, University of Brasília, 70910-900 Brasília, Brazil
[b] PPGCIMA, Campus Planaltina, University of Brasília, 73345-010 Brasília, Brazil

ARTICLE INFO

Keywords:
Janus-MoSSe
Aluminum-nitride
Interaction energy
Van der Waals Heterojunctions

ABSTRACT

The interaction mechanisms between Janus-MoSSe (MoSSe) and Aluminum-Nitride (AlN) sheets were systematically investigated by using Density Function Theory (DFT) calculations. Our computational protocol was based on performing single-point DFT calculations on AlN/MoSSe Van der Waals heterojunctions as a function of the distance between these two materials. Results show that the interaction energies vary from −35.5 up to −17.5 meV depending on the distance between the materials and the chemical species involved in the interface. The MoSSe/AlN heterojunctions, when the MoS face is interacting with the AlN sheet, presented the lowest interaction energies due to the sulfur's higher degree of reactivity.

1. Introduction

Due to the enormous growth in the global demand for energy consumption in the last decades, novel advances in renewable energy technologies have emerged recently [1–5]. In the establishment of these technologies, transition metal dichalcogenides (TMDs) have been playing an important role [6,7]. The most known TMD is the molybdenum disulfide (MoS_2), whose hexagonal monolayer (1H) phase is structurally similar to graphene [8,9]. One of the greatest advantages of MoS_2 in relation to graphene is its bandgap of 1.9 eV (1.3 eV) for monolayer (multilayer) phase [10,11]. These values are favorable for optical absorption when exposed to solar radiation [12–15]. In this sense, several works have been developed aiming at designing optoelectronic devices based on MoS_2 [16–20].

TMD-based heterostructures have been both theoretical and experimentally studied [21–26]. Recently, Janus-MoSSe-based heterostructures emerged as promising solutions for visible-infrared photocatalysis for water splitting [27–29] and metallic electrodes [30]. Importantly, is was experimentally reported that a Janus-MoSSe monolayer can be obtained through breaking the out-of-plane structural symmetry of the single-layer MoS_2[31]. In the yielded structure, the sulfur atoms on one side of the monolayer are fully replaced by the selenium ones [31]. Yin and coworkers theoretically studied the role of the intrinsic dipole on photocatalytic water splitting for Janus-MoSSe/Nitrides heterostructures by employing Density Functional Theory (DFT) calculations [32]. Their results showed that MoSSe/XN (X = Al, Ga) configurations with a perfect match between the hexagonal rings are always more stable than other types of stacking regardless of possible atomic positions [32]. Zhao and Schwingenschlögl investigated the van der Waals heterostructures constructed from Janus-Mosse/Germanene through first-principles calculations [30]. The germanene layer was chosen as electrode since it is a Dirac metal with a perfect lattice match to MoSSe [30]. Their findings revealed that an n-type Schottky contact was formed for SeMoS/Ge and a p-type Schottky contact for SMoSe/Ge [30]. A transition from Schottky to Ohmic behavior occurs under tensile strain (∼ 4% for SeMoS/Ge, ∼ 8% for SMoSe/Ge), which was explained by modifications of the interface dipole [30]. Albeit relevant studies have been performed to propose feasible applications for Janus-MoSSe-based heterostructures, to the best of our knowledge, the fundamental properties of Janus-MoSSe/Nitrides, such as their energetic stabilization, remains not fully understood and the present study fills this gap.

In the present work, we employed DFT calculations to systematically study the energetic stabilization of Janus-MoSSe and Aluminum-Nitride (MoSSe/AlN) Van der Waals heterostructures. The computational protocol adopted here was based on performing single-point DFT calculations as a function of the distance between these two materials to obtain the equilibrium distance. After that, we calculated the band structure only for the heterojuntions in their equilibrium distance (lowest

* Corresponding author at: Institute of Physics, University of Brasília, 70910-900 Brasília, Brazil.
E-mail address: ribeirojr@unb.br (L.A. Ribeiro).

https://doi.org/10.1016/j.cplett.2021.138465
Received 28 August 2020; Received in revised form 18 January 2021; Accepted 16 February 2021
Available online 10 March 2021
0009-2614/© 2021 Elsevier B.V. This article is made available under the Elsevier license (http://www.elsevier.com/open-access/userlicense/1.0/).

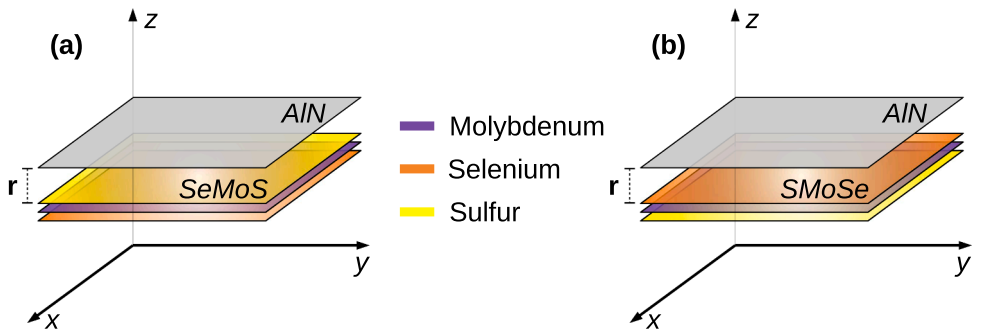

Fig. 1. Schematic representation for the stacking configuration of the (a) SeMoS/AlN (b) SMoSe/AlN heterojunctions. In this figure, *r* represents the distance between the AlN and TMD sheets.

interaction energies). Finally, *ab initio* molecular dynamics (MD) simulations were performed to attest to the stability of the MoSSe/AlN Van der Waals heterojunctions. Here, we considered four distinct assemblies (see Fig. 2)) to compose these heterojunctions. In the arranged the AlN and MoSSe sheets to allow the interaction between the MoS and MoSe faces with the AlN sheet. The results presented here shed light on the role played by Janus-MoSSe layers in stabilizing nitrides heterostructures.

2. Methodology

To investigate the structural and electronic properties of MoSSe/AlN heterostructures, we employed DFT calculations as implemented in the SIESTA package [33]. Within the framework of SIESTA, we used the numerical DZP basis set to expand the system wave functions of many atoms [34–36]. The exchange–correlation energies were calculated by using the Local Density Approximation (LDA), as proposed for Ceperley-Alder and Perdew-Wiang (LDA/CA and LDA/PW92, respectively) [37], and the Generalized Gradient Approximation (GGA), as proposed for Perdew-Burke-Ernzerhof and Perdew-Wiang (GGA/PBE, GGA/PW91, respectively) [38]. The relativistic pseudopotentials were parameterized within the Troullier-Martins formalism [39,40]. These approximations are required to describe the magnetic and electronic properties of materials composed of atoms with many electrons, as is the case of transition metals. A mesh cutoff of 400 Ry is chosen as a parameter for our calculations. The supercells containing MoSSe/AlN were previously converged, with a force criterion of 0.001 eV/Å, to fit in the box that was maintained orthogonal during all optimization. To calculate the bands an MPK mesh of $9 \times 9 \times 3$ was used [41].

The following equation was used to describe the interaction energy (E_I)

$$E_I(r) = E_{\mathrm{AlN}}^{\mathrm{MoSSe}}(r) - E_{\mathrm{AlN}} - E_{\mathrm{MoSSe}}, \quad (1)$$

where $E_{\mathrm{AlN}}^{\mathrm{MoSSe}}(r)$ is the energy of the MoSSe/AlN system that depends on the distance between the two monolayers. E_{AlN} and E_{MoSSe} are the energy of the isolated AlN monolayer and the isolated MoSSe monolayer, respectively. Importantly, *ab initio* molecular dynamics simulations were also performed, using the SIESTA code, to study the thermodynamical stability of the MoSSe/AlN heterostructures. These simulations were performed using an NPT ensemble with an initial/target temperature set to 300 K and a time-step of 3 fs.

Our computational protocol employed to study to predict the energetic stability of MoSSe/AlN Van der Waals heterostructures can be described in four stages: (1) we initially stacked the MoSSe and AlN sheets, separating them vertically by 5.0 Å, forming two distinct interfaces SeMoS/AlN (where the sulfur atoms are interacting with the AlN plane) and SMoSe/AlN (where the selenium atoms are interacting with the AlN plane), as represented in Fig. 1; (2) the AlN plane was translated towards the MoSSe one with a step of 0.1 Å and an interaction energy curves were obtained by performing single-point DFT calculations for each distance; (3) from the interaction energy curves, we obtained the equilibrium distances (or equivalently lowest interaction energies) related to the heterojunction arrangement that is more energetically stable; (4) after that, we calculated the band structure for the SMoSe and SeMoS heterojunctions in their equilibrium distances to describe their electronic structure; (4) in the last stage, *ab initio* molecular dynamics simulations were performed to attest the stability of the composed heterojunctions.

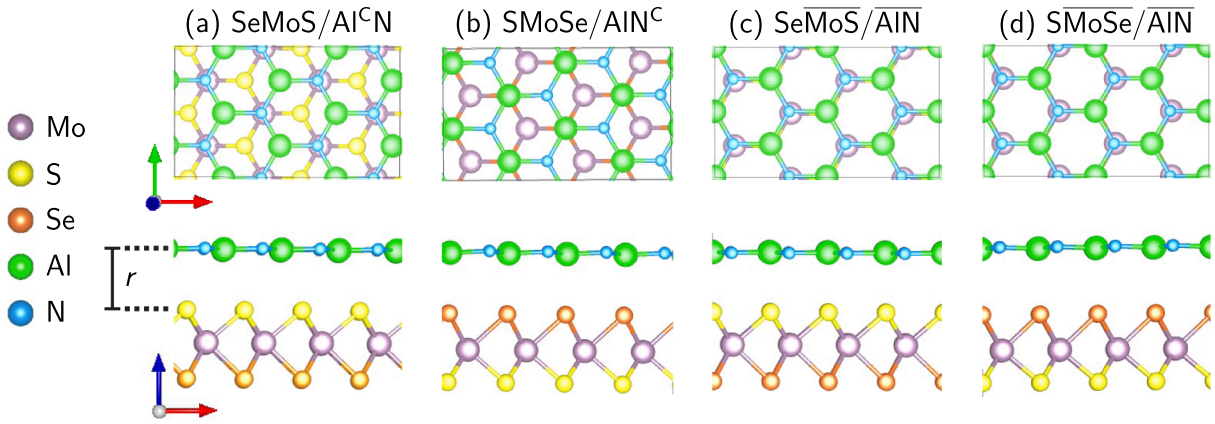

Fig. 2. Schematic representation of the four different cases considered in our simulations: (a) SeMoS/Al^{C}N (S-AlN interface), (b) SMoSe/AlN^{C} (Se-AlN interface), (c) Se$\overline{\mathrm{MoS}}$/$\overline{\mathrm{AlN}}$ (S-AlN interface), and (d) S$\overline{\mathrm{MoSe}}$/$\overline{\mathrm{AlN}}$ (Se-AlN interface), where N^{C} (Al^{C}) and $\overline{\mathrm{AlN}}$ denote a configuration in which the nitrogen (aluminium) is placed in the center of the TMD hexagons and the nitrogen is placed vertically aligned with the molybdenum atoms, respectively.

Table 1
Bond-length values were obtained here for the optimized MoSSe and AlN structures. Importantly, the values presented here are in good agreement with related ones reported in the literature [32].

Bond Type	SeMoS/Al^{C}N	SMoSe/AlN^{C}	Se$\overline{\text{MoS}}$/$\overline{\text{AlN}}$	S$\overline{\text{MoSe}}$/$\overline{\text{AlN}}$
Mo-S (Å)	2.39	2.42	2.39	2.39
Mo-Se (Å)	2.50	2.51	2.50	2.48
S-Se (Å)	3.25	3.26	3.26	3.21
Al-N (Å)	1.82	1.85	1.81	1.83

3. Results

We begin our discussion by presenting the different MoSSe/AlN systems investigated here as well as the protocol used to obtain their most stable heterojunctions. In Fig. 2 we illustrate the four different cases considered in our simulations: 2(a) SeMoS/Al^{C}N (S-AlN interface), 2(b) SMoSe/AlN^{C} (Se-AlN interface), 2(c) Se$\overline{\text{MoS}}$/$\overline{\text{AlN}}$ (S-AlN interface), and 2(d) S$\overline{\text{MoSe}}$/$\overline{\text{AlN}}$ (Se-AlN interface), where N^{C} (Al^{C}) and $\overline{\text{N}}$ denote a configuration in which the nitrogen (aluminum) atoms are localized in the center of the TMD hexagons and the nitrogen atoms are vertically aligned with the molybdenum ones, respectively. These model supercells have the following dimensions: 2(a) 10.87 × 6.30 × 49.41 Å, 2(b) 10.04 × 6.40 × 38.86 Å, 2(c) 10.86 × 6.29 × 49.51 Å, and 2(d) 10.89 × 6.31 × 39.9 Å. Importantly, the bond-length values obtained here for the optimized structures (see Table 1) are in good agreement with the ones reported in literature [32]. In our computational protocol to predict the most stable heterojunction (with lowest stabilization energy), we performed a systematic variation of the *r* distance (see Fig. 2) between the TMD and AlN surfaces from 1.9 up to 5.0 Å. The composite systems were initially optimized to adjust cell lengths and the TMD and AlN planes were separated from 3.5 Å. For each *r* distance, a single-point calculation was performed to obtain the interaction energy. Importantly, the four cases studied here (Fig. 2) are solutions of the geometry optimization procedure when the MoSSe and AlN sheets were positioned with/without matching their hexagonal rings. Moreover, *ab initio* MD simulations were also performed to verify the dynamical stability of the interfaces with lowest interaction energies.

The stabilization energy curves are shown in Fig. 3. These curves were obtained using the set of DFT functionals and potentials described in the previous section. In Fig. 3, one can note that the lowest E_P energy for the SeMoS/Al^{C}N, SMoSe/AlN^{C}, Se$\overline{\text{MoS}}$/$\overline{\text{AlN}}$, and S$\overline{\text{MoSe}}$/$\overline{\text{AlN}}$ cases is −4.66 meV (LDA/CA), −4.20 meV (LDA/CA), −5.41 meV (LDA/CA), and −5.50 meV (LDA/PW92), respectively. As expected, the cases with the lowest interaction energies are the ones in which the perfect match among the hexagons of both structures takes place (Se$\overline{\text{MoS}}$/$\overline{\text{AlN}}$ and S$\overline{\text{MoSe}}$/$\overline{\text{AlN}}$ cases). The cases where the sulfur atoms are interacting with the AlN surface (SeMoS/Al^{C}N and Se$\overline{\text{MoS}}$/$\overline{\text{AlN}}$) present the lowest interaction energies when contrasted to the selenium ones due to the higher degree of reactivity presented by silicon. Among all the heterostructures, the case with perpendicular configuration between sulfur-aluminum (Se$\overline{\text{MoS}}$/$\overline{\text{AlN}}$) presents the higher interaction energy than the related one with unpaired hexagons (SeMoS/Al^{C}N) due to the lower sulfur-aluminum distances.

To verify the suitability of the DFT methodologies employed here, we contrast the band structure profiles for the cases presented in Fig. 2, that were calculated using the methods described in the previous section. The band structures were obtained by considering the cases with the lowest interaction energies. One can note that all the DFT methodologies present very similar band structure profiles, as illustrated in Fig. 4. The bandgap values obtained using each one of them are presented in Table 2. They lie within the range of the visible spectrum and present a direct character between the Y and Γ points, making possible the photon absorption conserving electron momentum. Importantly, the calculated bandgap values (E_{gap}) ranged within the interval 1.61–1.87 eV, which can be interesting for photovoltaic applications.

To validate the thermodynamical stability of the MoSSe/AlN heterostructures studied here, we performed *ab initio* MD simulations, in which we considered as input the structures with the lowest interaction energies (also keeping the related DFT method). In this sense, Fig. 5 shows the time evolution of the total potential energy for each system. One can note that the potential energy remains constant during the time.

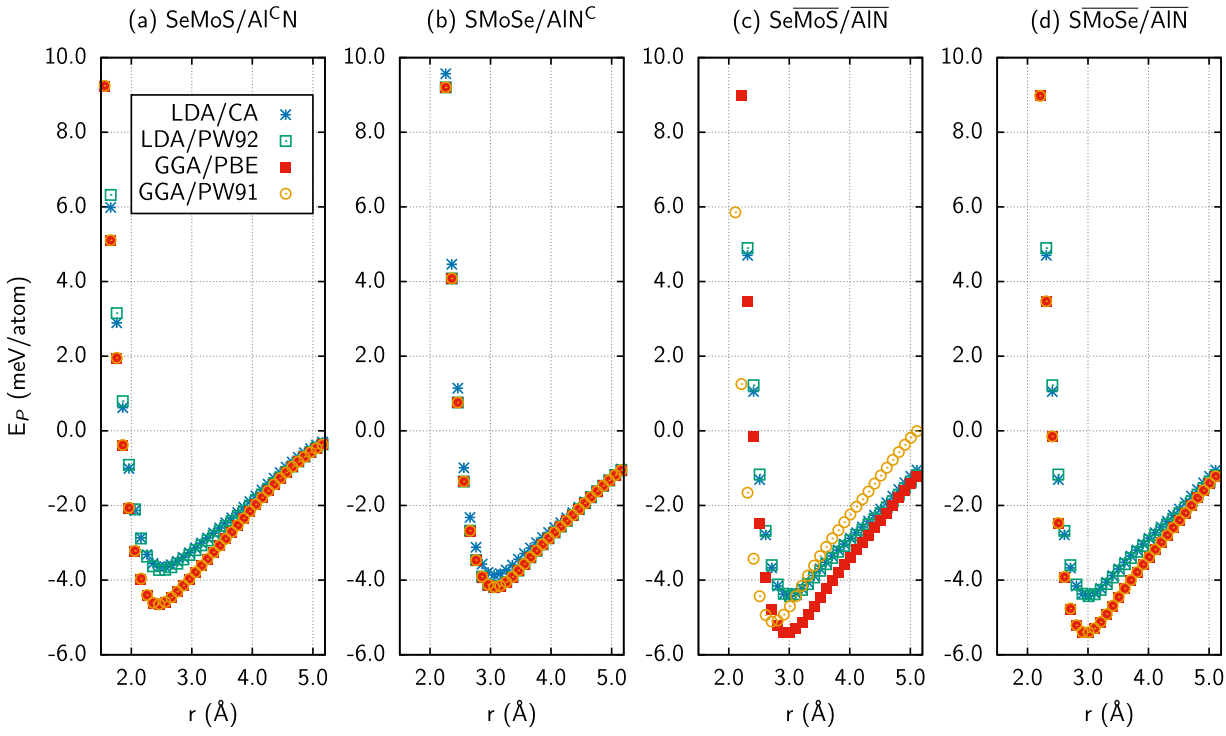

Fig. 3. Stabilization energy curves obtained using the set of DFT functionals and potentials described in the previous section.

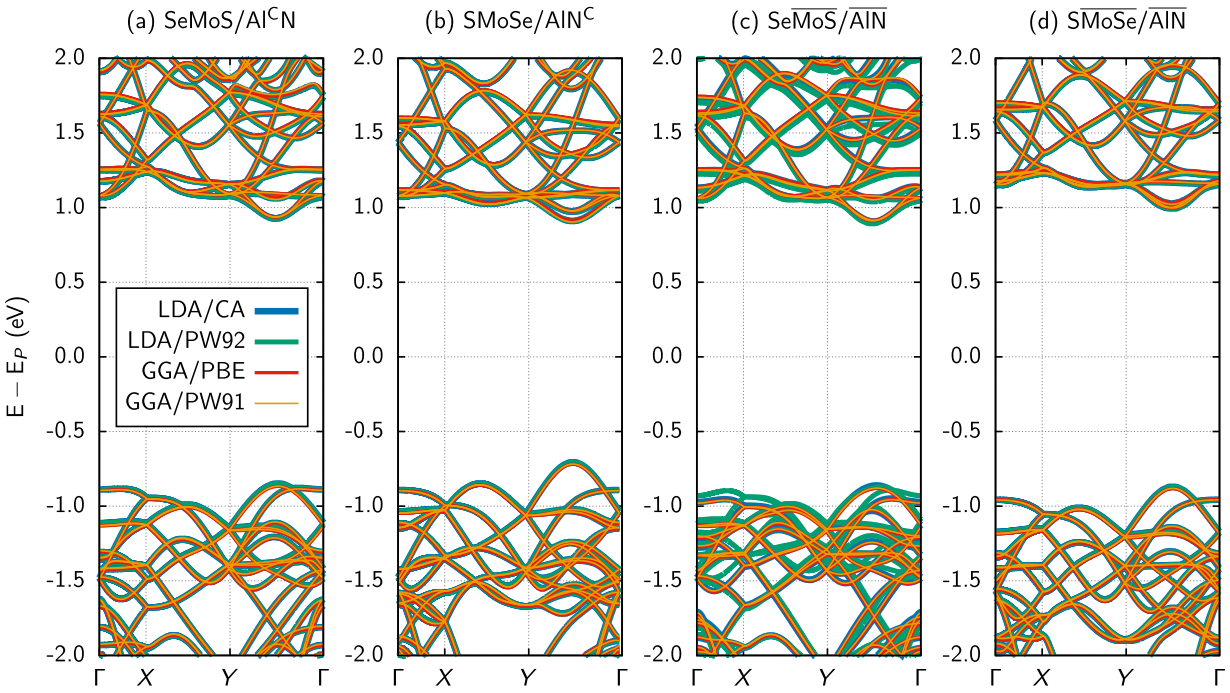

Fig. 4. Band structure profiles for the cases presented in Fig. 2 that were obtained using the different DFT methodologies described in the previous section.

Table 2
Bandgap values obtained for all the DFT methodologies used here. These values are related to the cases with the lowest interaction energies.

DFT Method	SeMoS/Al^{C}N	SMoSe/AlN^{C}	Se$\overline{\text{MoS}}$/$\overline{\text{AlN}}$	S$\overline{\text{MoSe}}$/$\overline{\text{AlN}}$
LDA/CA – E_{gap} (eV)	1.78	1.62	1.76	1.86
LDA/PW92 – E_{gap} (eV)	1.78	1.61	1.76	1.87
GGA/PBE – E_{gap} (eV)	1.80	1.62	1.79	1.87
GGA/PW91 – E_{gap} (eV)	1.80	1.61	1.80	1.87

As expected, the systems with lowest potential energies are the ones with a perfect match among the hexagonal rings of both structures (Se$\overline{\text{MoS}}$/$\overline{\text{AlN}}$ and S$\overline{\text{MoSe}}$/$\overline{\text{AlN}}$ cases), since they present the lowest interaction energies (Fig. 3). The *ab initio* MD results suggest that the interaction between MoSSe and AlN layers can yield stable heterostructures. It is worthwhile to stress that these results are in good agreement with the ones reported in literature [32], which showed that MoSSe/XN (X = Al, Ga) configurations with a perfect match between the hexagonal rings are always more stable than other types of stacking regardless of possible atomic positions.

4. Conclusions

In summary, we used DFT calculations to theoretically investigate the stacking mechanism of MoSSe/AlN heterostructures. The computational protocol employed here was based on single-point calculations and *ab inito* MD simulations to predict the interaction energies of van der Waals heterostructures constructed from MoSSe, where both the MoS and MoSe faces interacted with the AlN sheet. The results revealed that the stabilization (stacking) energies vary from −35.5 up to −17.5 meV depending on the chemical species involved in the interface. The lowest interaction energy for the SeMoS/Al^{C}N, SMoSe/AlN^{C}, Se$\overline{\text{MoS}}$/$\overline{\text{AlN}}$, and S$\overline{\text{MoSe}}$/$\overline{\text{AlN}}$ cases is −4.66 meV, −4.20 meV, −5.41 meV, and −5.50 meV, respectively. The cases with the lowest interaction energy are the ones in which the perfect match among the hexagons of both structures takes place (Se$\overline{\text{MoS}}$/$\overline{\text{AlN}}$ and S$\overline{\text{MoSe}}$/$\overline{\text{AlN}}$ cases). The cases where the sulfur atoms are interacting with the AlN surface (SeMoS/Al^{C}N and Se$\overline{\text{MoS}}$/$\overline{\text{AlN}}$) present the lowest interaction energy when contrasted to the selenium ones due to the higher degree of reactivity presented by silicon. Importantly, all the DFT methodologies used here presented similar band structure profiles. The bandgap values are in the range of 1.61–1.87 eV (visible spectrum) with a direct character. These band structure features can be interesting for photovoltaic applications. Moreover, *ab initio* MD simulations were performed to validate the thermodynamical stability of the MoSSe/AlN heterostructures studied here. In these simulations, the total potential energies remained constant during the time. Particularly, these results suggest that the interaction between MoSSe and AlN layers can yield stable heterostructures.

CRediT authorship contribution statement

Ramiro M. dos Santos: Data curation, Formal analysis, Methodology, Writing - original draft. **Marcelo L. Pereira Júnior:** Data curation, Formal analysis, Methodology, Writing - original draft. **Luiz F. Roncaratti:** Data curation, Formal analysis, Methodology, Writing - original draft. **Luiz A. Ribeiro Júnior:** Conceptualization, Supervision, Funding acquisition, Writing - review & editing.

Declaration of Competing Interest

The authors declare that they have no known competing financial interests or personal relationships that could have appeared to influence the work reported in this paper.

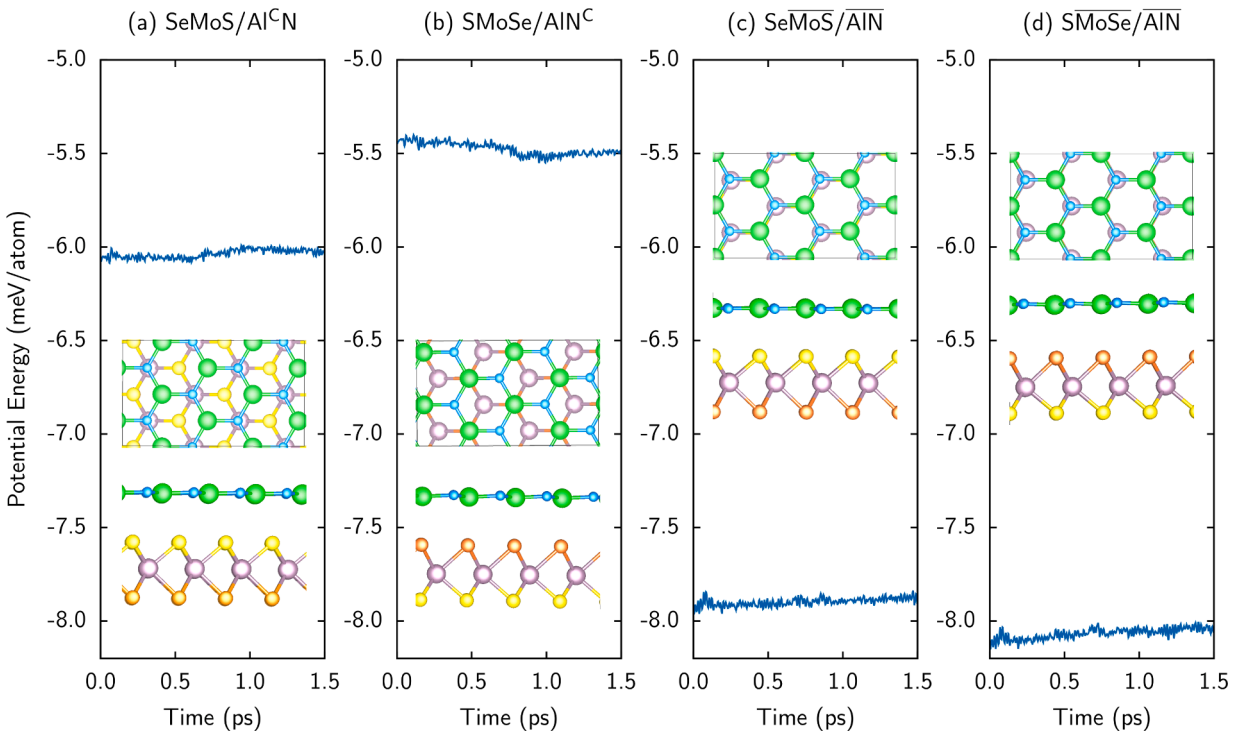

Fig. 5. Potential energy as a function of the time obtained in the *ab initio* MD simulations that considered as input the structures with the lowest interaction energies (also keeping the related DFT method).

Acknowledgments

The authors gratefully acknowledge the financial support from Brazilian research agencies CAPES, CNPq, FAPESP, and FAP-DF. M. L. P. J. gratefully acknowledges the financial support from CAPES grant 88882.383674/2019–01. L.A.R.J. gratefully acknowledges the financial support from CNPq grant 302236/2018–0 and the financial support from FAP-DF grant 0193.0000248/2019 −32. L.A.R.J. gratefully acknowledges the financial support from DPI/DIRPE/UnB (Edital DPI/DPG 03/2020) grant 23106.057541/2020 −89 and from IFD/UnB (Edital 01/2020) grant 23106.090790/2020 −86.

References

[1] Martin A. Green, Third generation photovoltaics: solar cells for 2020 and beyond, Physica E 14 (1–2) (2002) 65–70.
[2] Arthur J. Nozik, Matthew C. Beard, Joseph M. Luther, Matt Law, Randy J. Ellingson, Justin C. Johnson, Semiconductor quantum dots and quantum dot arrays and applications of multiple exciton generation to third-generation photovoltaic solar cells, Chem. Rev. 110 (11) (2010) 6873–6890.
[3] Gavin Conibeer, Martin Green, Richard Corkish, Young Cho, Eun-Chel Cho, Chu-Wei Jiang, Thipwan Fangsuwannarak, Edwin Pink, Yidan Huang, Tom Puzzer, et al., Silicon nanostructures for third generation photovoltaic solar cells, Thin Solid Films 511 (2006) 654–662.
[4] Norasikin A. Ludin, A.M. Al-Alwani Mahmoud, Abu Bakar Mohamad, H. Abd Amir Kadhum, Kamaruzzaman Sopian, Nor Shazlinah Abdul Karim, Review on the development of natural dye photosensitizer for dye-sensitized solar cells, Renew. Sustain. Energy Rev. 31 (2014) 386–396.
[5] Albert Polman, Harry A. Atwater, Photonic design principles for ultrahigh-efficiency photovoltaics, Nature Mater. 11 (3) (2012) 174–177.
[6] Meng-Lin Tsai, Su. Sheng-Han, Jan-Kai Chang, Dung-Sheng Tsai, Chang-Hsiao Chen, Wu. Chih-I, Lain-Jong Li, Lih-Juann Chen, Jr-Hau He, Monolayer mos2 heterojunction solar cells, ACS Nano 8 (8) (2014) 8317–8322.
[7] Sungjin Wi, Hyunsoo Kim, Mikai Chen, Hongsuk Nam, L Jay Guo, Edgar Meyhofer, and Xiaogan Liang. Enhancement of photovoltaic response in multilayer mos2 induced by plasma doping. ACS Nano 8(5) (2014) 5270–5281.
[8] Lakshay Dheer, Satadeep Bhattacharjee, Seung Cheol Lee, Umesh V Waghmare, Van der waals hetero-structures of 1h-mos2 and n-substituted graphene for catalysis of hydrogen evolution reaction, Mater. Res. Exp. 6 (12) (2020) 124006.
[9] Wenyan Zan, Wei Geng, Huanxiang Liu, Xiaojun Yao, Influence of interface structures on the properties of molybdenum disulfide/graphene composites: A density functional theory study, J. Alloy. Compd. 649 (2015) 961–967.
[10] Andrea Splendiani, Liang Sun, Yuanbo Zhang, Tianshu Li, Jonghwan Kim, Chi-Yung Chim, Giulia Galli, Feng Wang, Emerging photoluminescence in monolayer mos2, Nano Lett. 10 (4) (2010) 1271–1275.
[11] Philipp Tonndorf, Robert Schmidt, Philipp Böttger, Xiao Zhang, Janna Börner, Andreas Liebig, Manfred Albrecht, Christian Kloc, Ovidiu Gordan, Dietrich RT Zahn, et al. Photoluminescence emission and raman response of monolayer mos 2, mose 2, and wse 2. Opt. Exp. 21(4) (2013) 4908–4916.
[12] Yuanxin Li, Ningning Dong, Saifeng Zhang, Xiaoyan Zhang, Yanyan Feng, Kangpeng Wang, Long Zhang, Jun Wang, Giant two-photon absorption in monolayer mos2, Laser Photon. Rev. 9 (4) (2015) 427–434.
[13] A Steinhoff, J-H Kim, F Jahnke, M Rösner, D-S Kim, Ch Lee, Gang Hee Han, Mun Seok Jeong, TO Wehling, C. Gies, Efficient excitonic photoluminescence in direct and indirect band gap monolayer mos2, Nano Lett. 15(10) (2015) 6841–6847.
[14] Eric Singh, Ki Seok Kim, Geun Young Yeom, Hari Singh Nalwa, Atomically thin-layered molybdenum disulfide (mos2) for bulk-heterojunction solar cells, ACS Appl. Mater. Interfaces 9 (4) (2017) 3223–3245.
[15] Meng-Lin Tsai, Su. Sheng-Han, Jan-Kai Chang, Dung-Sheng Tsai, Chang-Hsiao Chen, Wu. Chih-I, Lain-Jong Li, Lih-Juann Chen, Jr-Hau He, Monolayer mos2 heterojunction solar cells, ACS Nano 8 (8) (2014) 8317–8322.
[16] Zongyou Yin, Hai Li, Hong Li, Lin Jiang, Yumeng Shi, Yinghui Sun, Lu. Gang, Qing Zhang, Xiaodong Chen, Hu.a. Zhang, Single-layer mos2 phototransistors, ACS Nano 6 (1) (2012) 74–80.
[17] Yexin Deng, Zhe Luo, Nathan J. Conrad, Han Liu, Yongji Gong, Sina Najmaei, Pulickel M. Ajayan, Jun Lou, Xianfan Xu, Peide D. Ye, Black phosphorus–monolayer mos2 van der waals heterojunction p–n diode, ACS Nano 8 (8) (2014) 8292–8299.
[18] Fengping Li, Wei Wei, Pei Zhao, Baibiao Huang, Ying Dai, Electronic and optical properties of pristine and vertical and lateral heterostructures of janus mosse and wsse, J. Phys. Chem. Lett. 8 (23) (2017) 5959–5965.
[19] Deependra Kumar Singh, Rohit Pant, Arun Malla Chowdhury, Basanta Roul, Karuna Kar Nanda, Saluru Baba Krupanidhi, Defect-mediated transport in self-powered, broadband, and ultrafast photoresponse of a mos2/aln/si-based photodetector. ACS Appl. Electron. Mater. 2(4) (2020) 944–953.
[20] Xiaobin Liao, Yunlong Zhao, Junhui Wang, Wei Yang, Lin Xu, Xiaocong Tian, Yi Shuang, Kwadwo Asare Owusu, Mengyu Yan, Liqiang Mai, Mos 2/mno 2 heterostructured nanodevices for electrochemical energy storage, Nano Res. 11(4) (2018) 2083–2092.
[21] eljko ljivananin, Milivoj Beli, Graphene/mos_2 heterostructures as templates for growing two-dimensional metals: Predictions from ab initio calculations, Phys. Rev. Mater. 1 (2017) 044003.
[22] Dongyuan Chen, Weixiang Chen, Lin Ma, Ge Ji, Kun Chang, Jim Yang Lee, Graphene-like layered metal dichalcogenide/graphene composites: synthesis and applications in energy storage and conversion, Mater. Today 17 (4) (2014) 184–193.
[23] Georg Duesberg, Heterojunctions in 2d semiconductors: A perfect match, Nature Mater. 13 (2014) 1075–1076.

[24] Miguel M. Ugeda, Aaron J. Bradley, Su-Fei Shi, H. Felipe, Yi Zhang, Diana Y. Qiu, Wei Ruan, Sung-Kwan Mo, Zahid Hussain, Zhi-Xun Shen, et al. Giant bandgap renormalization and excitonic effects in a monolayer transition metal dichalcogenide semiconductor, Nature Mater. 13(12) (2014) 1091–1095.
[25] Martin Gmitra, Jaroslav Fabian, Graphene on transition-metal dichalcogenides: A platform for proximity spin-orbit physics and optospintronics, Phys. Rev. B 92 (2015) 155403.
[26] Amin Azizi, Sarah Eichfeld, Gayle Geschwind, Kehao Zhang, Bin Jiang, Debangshu Mukherjee, Lorraine Hossain, Aleksander F. Piasecki, Bernd Kabius, Joshua A. Robinson, et al., Freestanding van der waals heterostructures of graphene and transition metal dichalcogenides. ACS Nano 9(5) (2015) 4882–4890.
[27] Lin Ju, Mei Bie, Jing Shang, Xiao Tang, Liangzhi Kou, Janus transition metal dichalcogenides: superior platform for photocatalytic water-splitting, J. Phys.: Mater. 3 (2020).
[28] Xu. Yimin, Yongsheng Yao, Wenjin Yin, Juexian Cao, Mingyang Chen, Xiaolin Wei, Intrinsic defect engineered janus mosse sheet as a promising photocatalyst for water splitting, RSC Adv. 10 (18) (2020) 10816–10825.
[29] M. Idrees, H.U. Din, Shafiq Ur Rehman, M. Shafiq, Yasir Saeed, H.D. Bui, Chuong V Nguyen, Bin Amin, Electronic properties and enhanced photocatalytic performance of van der waals heterostructures of zno and janus transition metal dichalcogenides, Phys. Chem. Chem. Phys. 22 (18) (2020) 10351–10359.
[30] Ning Zhao, Udo Schwingenschlögl, Transition from schottky to ohmic contacts in janus mosse/germanene heterostructures, Nanoscale 12 (2020) 11448–11454.
[31] Lu. Ang-Yu, Hanyu Zhu, Jun Xiao, Chih-Piao Chuu, Yimo Han, Ming-Hui Chiu, Chia-Chin Cheng, Chih-Wen Yang, Kung-Hwa Wei, Yiming Yang, et al., Janus monolayers of transition metal dichalcogenides, Nature Nanotechnol. 12 (8) (2017) 744–749.
[32] Wenjin Yin, Bo Wen, Qingxia Ge, Daifeng Zou, Ying Xu, Mingwei Liu, Xiaolin Wei, Mingyang Chen, Xiaoli Fan, Role of intrinsic dipole on photocatalytic water splitting for janus mosse/nitrides heterostructure: A first-principles study, Prog. Natural Sci.: Mater. Int. 29(3) (2019) 335–340. Special Issue of Computational Materials.
[33] José M. Soler, Emilio Artacho, Julian D. Gale, Alberto García, Javier Junquera, Pablo Ordejón, Daniel S.ánchez-Portal, The SIESTA method forab initioorder-nmaterials simulation, J. Phys.: Condens. Matter 14(11) (2002) 2745–2779.
[34] W. Kohn, L.J. Sham, Self-consistent equations including exchange and correlation effects, Phys. Rev. 140 (1965) A1133–A1138.
[35] P. Hohenberg, W. Kohn, Inhomogeneous electron gas, Phys. Rev. 136 (1964) B864–B871.
[36] James P. Lewis, Kurt R. Glaesemann, Gregory A. Voth, Jürgen Fritsch, Alexander A. Demkov, José Ortega, Otto F. Sankey, Further developments in the local-orbital density-functional-theory tight-binding method, Phys. Rev. B 64 (2001) 195103.
[37] David C. Langreth, M.J. Mehl, Beyond the local-density approximation in calculations of ground-state electronic properties, Phys. Rev. B 28 (1983) 1809–1834.
[38] John P. Perdew, Kieron Burke, Matthias Ernzerhof, Generalized gradient approximation made simple, Phys. Rev. Lett. 77 (1996) 3865–3868.
[39] Warren E. Pickett, Pseudopotential methods in condensed matter applications, Comput. Phys. Rep. 9 (3) (1989) 115–197.
[40] N. Troullier, José Luís Martins, Efficient pseudopotentials for plane-wave calculations. ii. operators for fast iterative diagonalization, Phys. Rev. B 43 (1991) 8861–8869.
[41] Hendrik J. Monkhorst, James D. Pack, Special points for brillouin-zone integrations, Phys. Rev. B 13 (1976) 5188–5192.